Measuring binding kinetics of surface-bound molecules using the surface plasmon resonance technique

Baoxia Li, Juan Chen, Mian Long *

National Microgravity Laboratory and Center of Biomechanics and Bioengineering, Institute of Mechanics, Chinese Academy of Sciences, Beijing 100190, Peoples Republic of China

ARTICLE INFO

ABSTRACT

Surface plasmon resonance (SPR) technology and the Biacore biosensor have been widely used to measure the kinetics of biomolecular interactions in the fluid phase. In the past decade, the assay was further extended to measure reaction kinetics when two counterpart molecules are anchored on apposed surfaces. However, the cell binding kinetics has not been well quantified. Here we report development of a cellular kinetic model, combined with experimental procedures for cell binding kinetic measurements, to predict kinetic rates per cell. Human red blood cells coated with bovine serum albumin and anti-BSA monoclonal antibodies (mAbs) immobilized on the chip were used to conduct the measurements. Sensorgrams for BSA-coated RBC binding onto and debinding from the anti-BSA mAb-immobilized chip were obtained using a commercial Biacore 3000 biosensor, and analyzed with the cellular kinetic model developed. Not only did the model fit the data well, but it also predicted cellular on and off-rates as well as binding affinities from curve fitting. The dependence of flow duration, flow rate, and site density of BSA on binding kinetics was tested systematically, which further validated the feasibility and reliability of the new approach.

Crown copyright © 2008 Published by Elsevier Inc. All rights reserved.

The Biacore biosensor is an optical device used to determine biomolecular interactions between immobilized ligands or antibodies and flowing receptors or antigens in real time [1–3]. With surface plasmon resonance (SPR)[1] technology, it measures the changes in refractive index near a planar chip surface (within a distance of ~300 nm from the surface) induced by binding of soluble molecules to immobilized counterpart molecules on the sensor chip. Kinetic rates and equilibrium affinity of biomolecular interactions are then predicted by fitting measured data (sensorgrams) using reaction kinetic models in bulk chemistry. The Biacore biosensor together with relevant analyses has become a widely used standard method for characterizing biomolecular interactions in laboratories and in the food and pharmaceutical industries [4–6]. Much effort has been focused on providing accurate and reliable data, improving data analysis, and widening the applications [1,7–9].

Recently, SPR technology and the Biacore biosensor were further extended to measure the interactions of biomolecules expressed on the surface of a cell, virus, or particle, which enables direct determination of the binding of surface-bound molecules without protein purification and/or reconstruction. For example,

binding of human red blood cells (RBCs) expressing blood group antigens to immobilized anti-blood group-specific antibodies on the Biacore chip surface has been measured to sort blood group-specific RBCs from whole blood samples [10,11]. Similar tests were done to characterize some novel monoclonal antibodies (mAbs) to virulent *Listeria monocytogenes* cells [12], to screen peptide ligands selectively capturing circulating malignant epithelial cells from human prostate, bladder, and breast cancer cells [13], to map binding epitopes in the *Plasmodium vivax* domain that adhere to Duffy antigen in RBC invasion [14], to determine the valency of antibody binding to enveloped human influenza virus particles [4], and to measure the binding of *Staphylococcus aureus* and *Staphylococcus epidermidis* cells to immobilized fibronectin [15]. Technically, four SPR-based biosensors were proposed, in which a commercialized Biacore biosensor enables cell binding measurements at the lowest nonspecific binding [11]. Although previous studies have offered the potential to extend SPR-based Biacore biosensor in measuring biomolecular interactions on the cell surface, quantitative analyses of kinetic rates and binding affinity remain lacking.

In a Biacore biosensor, binding of flowing cells to immobilized probes on the chip is mediated by underlying antibody–antigen or receptor–ligand interactions, which are governed by kinetic rates and binding affinity, as well as site densities of surface-bound molecules, cell concentration, flow rate, and flow duration. For example, cell binding responses were enhanced when higher concentrations of flowing cells or higher site densities of immobilized

antibodies were used [4,10,15]. Low flow rate and long flow duration retain the same kinetics as high flow rate and short flow duration [15]. However, interpretation of binding data and calculation of kinetic rates and binding affinity become complicated because kinetic models used in bulk chemistry are unable to relate apparent cell binding responses to intrinsic kinetic parameters of the interacting molecular pair. Thus, development of a rationale for cellular and molecular kinetic models and relevant analyses to quantify biomolecular interactions on the cell surface is required.

Binding of soluble or cell-bound antigens (or receptor) to immobilized antibodies (or ligand) is governed by respective kinetic mechanisms. In contrast to three-dimensional (3D) binding where at least one of the two molecules is in fluid phase, the binding of cell-bound molecules to immobilized counterpart molecules requires that both molecules are captured on two apposed surfaces, so-called two-dimensional (2D) binding. In typical 3D binding as performed in conventional Biacore tests, mass transportation effect needs to be accounted for in best fitting sensorgram data at different receptor concentrations and ligand site densities in systematically varied flow rates when the reaction kinetics in bulk chemistry is applied to a large reaction system (say, analyte concentration > nanomolar) [7,16]. In 2D binding, however, a probabilistic model is required because the binding of a cell-bound antigen (or receptor) to an immobilized antibody (or ligand) is a stochastic process, which is governed by the 2D kinetics of small systems. Although the probabilistic model has been widely applied using different molecular systems in various assays [17–23], care should be taken when it is applied to quantify biomolecular interactions in a Biacore biosensor, where mass transportation of flowing cells and forced formation and dissociation of antigen–antibody (or receptor–ligand) bonds have great impact on cell binding responses [24,25]. As the first in a series of studies, we propose in the present work a cellular kinetic model that relates cell binding responses to cellular kinetic rates, and develop relevant procedures and approaches to conduct the measurements and analyze the data. The model not only fits sensorgram data well, but also enables prediction of the kinetic parameters of surface-bound biomolecular interactions.

Kinetic modeling

We developed a new kinetic model to quantify the 2D kinetics of interactions between a molecule (species A) and its counterpart molecule (species B). When binding of A molecules coupled to or expressed on a cell to B molecules immobilized on substrate is conducted in a Biacore biosensor (Fig. 1a), the reaction no longer follows 3D kinetics in bulk chemistry. Molecule-coupled or -expressed cells are driven to bind onto and debind from B molecule-immobilized substrate when flowing in the vicinity of the chip surface (~one cell height high from surface). Recorded time courses of response units (RU), or sensorgrams, represent the number of bound cells on the chip surface (Fig. 1b).

Cell binding and debinding are governed by 2D forward and reverse reactions between surface-bound interacting molecules. Here a cellular kinetic model is proposed to predict binding kinetics per cell from sensorgrams. Assuming that A and B molecules are uniformly distributed on cell and chip surfaces, respectively, and that binding of a cell to one region of chip surface does not affect the ability of another cell to adhere to another region on chip surface, cell binding and debinding kinetics is described in terms of effective on-rate K_{on}^{c} (in s^{-1}), and off-rate per cell k_{off}^{c} (in s^{-1}), respectively,

$$[\text{Cell}]_{\text{free}} \underset{k_{off}^{c}}{\overset{K_{on}^{c}}{\rightleftarrows}} [\text{Cell}]_{\text{Bound}} \tag{1}$$

where the reciprocals of effective on- and off-rates, $1/K_{on}^{c}$ and $1/k_{off}^{c}$, are defined as the respective characteristic time constants of free cells binding to and bound cells debinding from the surface. Specifically, the number of bound cells at time t, $N(t)$, during the cell suspension injection or association phase follows

$$\frac{dN(t)}{dt} = K_{on}^{c}[N_{max} - N(t)] - k_{off}^{c}N(t) \tag{2a}$$

or

$$\frac{d\text{RU}(t)}{dt} = K_{on}^{c}[\text{RU}_{max} - \text{RU}(t)] - k_{off}^{c}\text{RU}(t), \tag{2b}$$

where N_{max} is the maximum number of bound cells geometrically available at a given site density of B molecules on chip surface [10]. Eq. (2b) is obtained by assuming that the number of bound cells is linearly proportional to RU by a constant, k_{RU}, that is, $\text{RU}(t) = k_{RU} \times N(t)$ and $\text{RU}_{max} = k_{RU} \times N_{max}$ [10,26]. Integrating Eq. (2b) returns an analytical solution:

$$\text{RU}(t) = \frac{K_{on}^{c} \times \text{RU}_{max}}{K_{on}^{c} + k_{off}^{c}} \{1 - \exp[-(K_{on}^{c} + k_{off}^{c})t]\}. \tag{2c}$$

Note that $K_{on}^{c}(= k_{on}^{c} \times C)$ is a lumped kinetic parameter, where k_{on}^{c} (in $ml \cdot s^{-1}$) is the on-rate per cell, and C(in ml^{-1}) is the average number concentration of freely flowing cells close to surface. In the current work, K_{on}^{c} is used as a measure of association reaction as C is unable to be measured experimentally.

Assuming that detached cells are unable to rebind onto chip surface, the response unit for cells remaining bound at time t, $\text{RU}(t)$, during running buffer injection or dissociation phase, is

$$\frac{d\text{RU}(t)}{dt} = -k_{off}^{c}\,\text{RU}(t). \tag{3a}$$

Again, integrating Eq. (3a) yields an analytical solution,

$$\text{RU}(t) = \text{RU}^{p} \times \exp(-k_{off}^{c}t), \tag{3b}$$

where RU^{p} is the peak RU value at the end of the association phase.

To predict binding kinetic parameters, we use Eqs. (2c) and (3b) to fit independently the data for association and dissociation phases, respectively, from measured sensorgrams. This yields a set of lumped binding rates, $K_{b}^{c}(= K_{on}^{c} + k_{off}^{c})$, and off-rates per cell, k_{off}^{c}. We then calculate the effective on-rate per cell, K_{on}^{c} (=$K_{b}^{c} - k_{off}^{c}$), and effective binding affinity per cell, $K_{a}^{c}(= K_{on}^{c}/k_{off}^{c})$, from the above definitions. The statistical significance (or lack thereof) of the difference in RU^{p} values at different flow rates and durations or in kinetic rates at different flow rates was assessed using the Student t test.

Materials and methods

Biotinylation of BSA and RBCs

Bovine serum albumin (BSA) (Sigma, USA) was coupled to the surfaces of RBCs using a modified biotin–avidin–biotin linkage protocol [27–29]. Briefly, BSA proteins were biotinylated by incubating 2 mg of proteins with 0.25 mg of NHS-LC-Biotin for 1 h according to the manufacturer's instructions (EZ-Link, Pierce, USA). BSA:biotin ratio for biotinylated BSA or the number of biotin molecules per BSA molecule was then determined with the HABA kit (Pierce, USA), and was 1:20 in the current work.

RBCs were isolated from fresh whole blood of healthy donors, and washed three times in phosphate-buffered solution (PBS). Collected RBCs were then biotinylated by incubating 10^{9} RBCs with 100 mM sulfo-NHS-LC-Biotin for 45 min according to a modification of the manufacturer's instructions. After being rinsed, biotinylated RBCs were kept at 4 °C in RBC storage solution (EAS45+) [30,31].
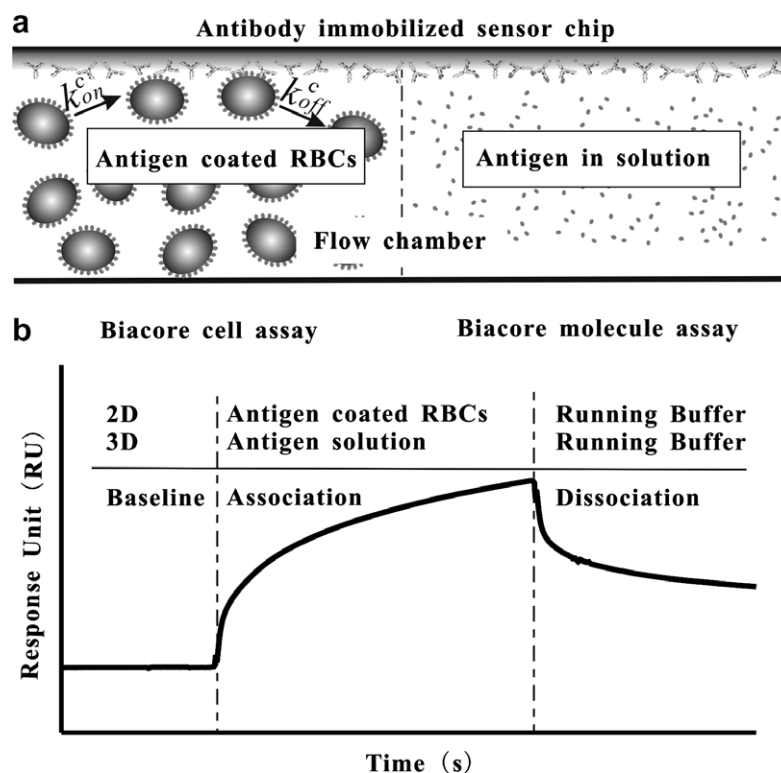
Fig. 1. Schematic of Biacore binding assay. (a) In the Biacore cell assay or 2D assay, antigen-expressed or –coupled RBCs are perfused into the flow chamber, where they interact with the antibody-immobilized chip surface (left). Also illustrated is the Biacore molecular assay or 3D assay, in which soluble antigens or analytes are perfused (right). Dimensions are not scaled. (b) Time course of response unit (RU) or sensorgram is demonstrated in terms of baseline, association, and dissociation phases.

BSA coupling on RBCs

Approximately 800 μl of biotinylated RBCs at 2.5×10^8 cells/ml was added into 200 μl of 1 mg/ml avidin solution, which was incubated at room temperature under mild agitation for 45 min to form a biotin–avidin complex on RBCs. Biotin–avidin-linked RBCs were washed three times and resuspended in 950 μl of PBS. Fifty microliters of biotinylated BSA at 10–100 μg/ml was then added into the suspension, which was incubated at room temperature under mild agitation for 45 min to couple BSA to RBCs. After being rinsed, BSA-coupled RBCs were kept at 4 °C in EAS45+.

Coupling efficiency and site density of BSA on RBCs were determined using flow cytometry. RBCs were incubated with fluorescein isothiocyanate-conjugated sheep anti-BSA monoclonal antibody (mAb) (Immunology Consultants Laboratory, Newberg, OR, USA) at a concentration of 10 μg/ml in 200 μl PBS buffer at 4 °C for 35 min. After being washed, the cells were analyzed by flow cytometry. Site densities were then calculated by comparing the fluorescence intensities of the cells with those of standard beads (Bangs Labs, Fishers, IN, USA) [20,23], which were 45 and 82 μm^{-2} in the current work.

Biacore cell assay

For this assay, 10 μg/ml of mouse anti-BSA mAb in 10 mM sodium acetate (pH 5.0) (Sigma, USA) was covalently coupled to the channels of CM5 chip surface with primary amine groups using a standard amine coupling method, which yielded ~9000 and ~12,000 RU. A plain channel subjected to the same activation and deactivation treatments but without immobilized proteins was used as the control.

Kinetic measurements were performed using the Biacore 3000 biosensor (Pharmacia, Sweden) at 25 °C on CM5 chip with PBS as running buffer (Fig. 1a). BSA-coated RBCs in filtered and degassed

EAS45 + at 4×10^7 cells/ml were fully premixed and injected to flow over the channels, followed by perfusing PBS, at preset flow durations and flow rates. Cell-bound chip surface was regenerated by perfusing PBS for a long time (>30 min) at a high flow rate (>50 μl/min). This test cycle of association, dissociation, and regeneration was repeated in triplicate in each condition. Time courses of cell binding responses (RU) were recorded in real time (Fig. 1b). Flow duration and flow rate were systematically varied in the ranges 10–15 min and 1–10 μl/min, respectively.

Results

Cell binding was specifically mediated by BSA–anti-BSA antibody interactions

Binding specificity of BSA-coupled RBCs to anti-BSA mAb-immobilized chip surface was quantified in terms of time dependence of cell binding responses, RU. As exemplified in Fig. 2, RU was dramatically higher when both BSA and anti-BSA mAbs were present (dashed line) than when anti-BSA mAbs were absent (dotted line). Similar nonspecific responses were also observed when BSA-coupled RBCs were preincubated with soluble anti-BSA mAbs before being injected into the flow chamber (data not shown). The time course of specific response, RU^S (solid line), was obtained by subtracting nonspecific response, RU^N, from total response, RU^T. These data demonstrated that cell binding measured using SPR technology and the Biacore 3000 biosensor was specifically mediated by BSA–anti-BSA mAb interactions.

Binding was regulated by flow duration and flow rate

Cell-specific responses, RU^S, are regulated by flow duration. To test this, flow duration was systematically varied at 10 and
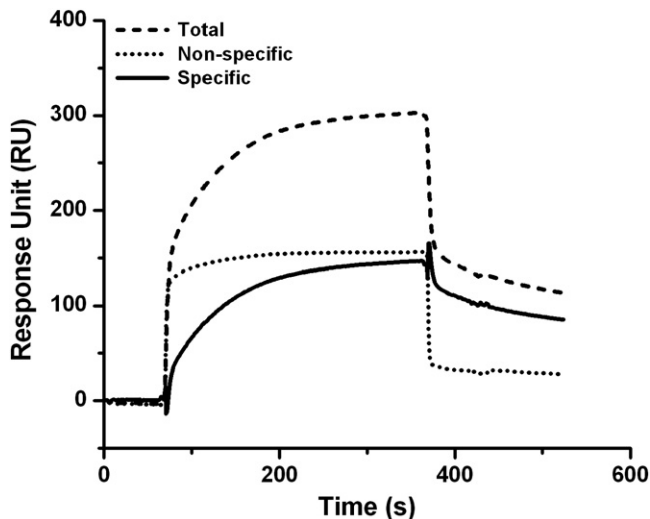
Fig. 2. Cell binding specificity. The response unit for specific binding of BSA–anti-BSA antibody interactions, RU^S (solid line), was obtained by subtracting nonspecific binding of BSA-coupled RBCs to plain chip surface, RU^N (dotted line), from total binding of BSA-coupled RBCs to anti-BSA mAb-immobolized chip surface, RU^T (dashed line).

15 min at preset flow rates. As exemplified in Fig. 3a, the binding of BSA-coupled RBCs at a given flow rate of 5 μl/min was significantly enhanced when flow duration was prolonged from 10 (gray dashed line) to 15 (gray dotted line) min. Similar dependences of flow duration were also observed at flow rates of 1 and 10 μl/min (data not shown). This was further confirmed by comparing RU^P at different flow durations. As shown in Fig. 3b, RU^P was 1.6-fold lower at 1 μl/min, 1.3-fold lower at 5 μl/min, and 1.3-fold lower at 10 μl/min, at 10 min (solid bars) than at 15 min (open bars). Dissociation of bound cells followed a similar debinding kinetics at various flow durations, suggesting that flow duration or reaction time would not influence dissociation kinetics.

Alternatively, cell-specific responses, RU^S, are regulated by flow rate. To conduct the test, flow rate was systematically varied for 1, 5, and 10 μl/min at preset flow durations. As exemplified in Fig. 4a, the binding of BSA-coupled RBCs at a given flow duration of 10 min was enhanced when flow rate increased from 1 (gray dashed line) to 5 (gray dotted line) and 10 (gray solid line) μl/min. Similar dependences of flow rate were also observed at a flow duration of 15 min (data not shown). RU^P was 1.7- and 1.9-fold lower at 10 min, and 1.3- and 1.5-fold lower at 15 min, respectively, at 1 μl/min (solid bars) than at 5 (open bars) and 10 μl/min (hatched bars) (Fig. 4b). Again, dissociation of bound cells followed a similar debinding kinetics at various flow durations, implying that flow rate or cell transportation would not influence dissociation kinetics.

Binding followed a simple kinetics

The time course measured for specific response, RU^S, exhibited an ascending transition phase when BSA-coupled RBCs were perfused into the flow chamber, as exemplified in Fig. 2 (solid line), 3a, and 4a, indicating that number of bound BSA-coupled RBCs was enhanced with flow duration. It was then followed by a descending transition phase when PBS was perfused, demonstrating that bound RBCs were reduced by buffer flow. Eqs. (2c) and (3b) were used to fit the association and dissociation phases in each curve, respectively, to obtain two parameters: K_b^c and k_{off}^c. The fitted K_b^c and k_{off}^c values were then used to predict each RU-versus-t curve (black solid lines in Figs. 3a and 4a). It is evident that
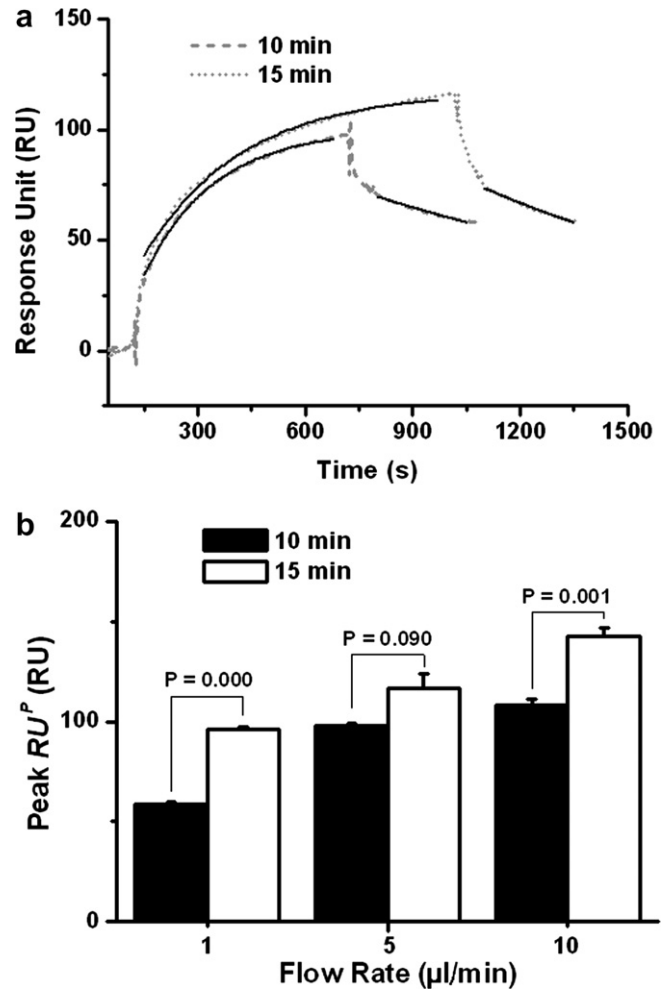

Fig. 3. Dependence of flow duration. (a) Plot of response unit against time at two flow durations of 10 min (gray dashed line), and 15 min (gray dotted line), at a given flow rate of 5 μl/min. Also plotted are the theoretical predictions using Eqs. (2c) and (3b) (black solid lines). (b) Peak response unit, RU^P, is plotted at 10 (solid bars) and 15 (open bars) min, at three given flow rates of 1, 5, and 10 μl/min. Data are presented as mean ± SE RU^P for three test cycles at that flow duration. The P value indicates the level of statistical significance of differences in peak RU^P at different flow durations.

the model fits the data well, imparting confidence in the estimated kinetic parameters.

Flow rate, but not flow duration, regulated cellular kinetic parameters

The impact of flow duration on the fitted kinetic parameters was tested using both individual and global fitting at a given flow rate of 5 μl/min. In an individual fitting, the data for three test cycles at each flow duration were pooled and fitted using Eqs. (2c) and (3b) to predict kinetic parameters at that flow duration, as exemplified in Fig. 5 at 10 (open bars) and 15 (solid bars) min, respectively, and the mean values were obtained by averaging the two sets of parameters (hatched bars). No marked differences in kinetic parameters were observed at the two flow durations ($K_b^c = 5.2 \times 10^{-3}$ and 3.6×10^{-3} s^{-1} at 10 and 15 min, respectively). This was further confirmed by a global fitting, where the data for all six test cycles at two flow durations were pooled and then fitted using the model to obtain a single set of parameters. Global fitting yielded a set of kinetic parameters of $K_b^c = 3.6 \times 10^{-3}$ and $k_{off}^c = 8.2 \times 10^{-4}$ s^{-1} (dotted bars), which was in excellent agreement with the mean of the parameters fitted
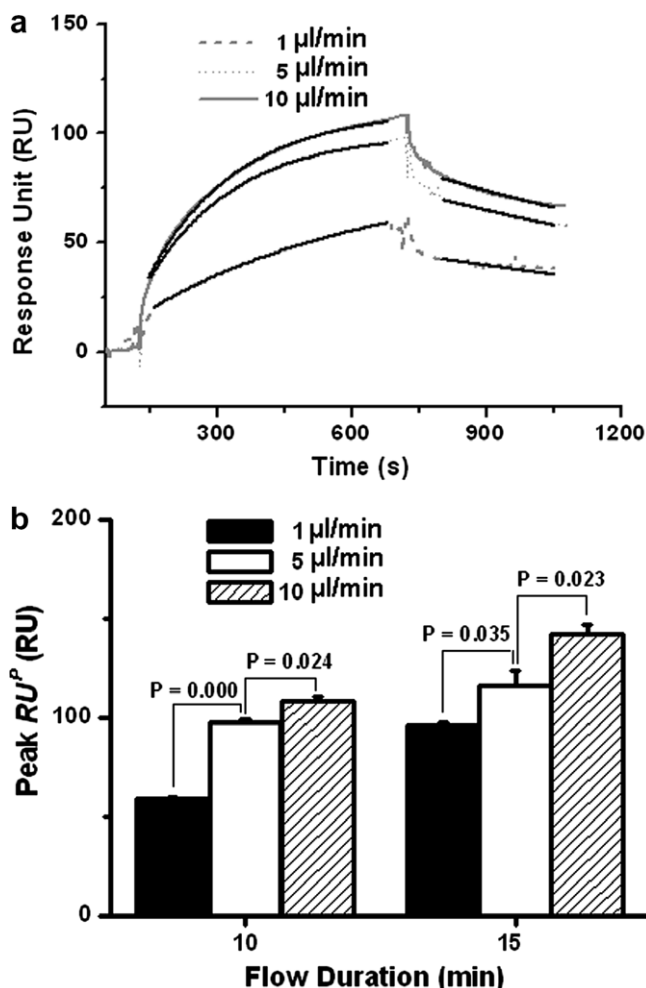
Fig. 4. Dependence of flow rate. (a) Plot of response unit against time at three flow rates of 1 (gray dashed line), 5 (gray dotted line), and 10 (gray solid line) μl/min, at a given flow duration of 10 min. Also plotted are the theoretical predictions using Eqs. (2c) and (3b) (black solid lines). (b) Peak response unit, RU^P, is plotted at 1 (solid bars), 5 (open bars), and 10 (hatched bars) μl/min, at two given flow durations of 10 and 15 min. Data are presented as mean ± SE RU^P for three test cycles at that flow rate. The P value indicates the level of statistical significance of differences in peak RU at different flow rates.

Fig. 5. Dependence of cellular kinetic rates on flow duration at a given flow rate of 5 μl/min. Lumped binding rate, K_b^c, and off-rate per cell, k_{off}^c, are obtained by fitting individually the measured sensorgrams using Eqs. (2c) and (3b) at 10 (open bars) and 15 (solid bars) min. Also plotted are the mean values obtained by averaging the two sets of parameters predicted from individual fitting at each flow duration (hatched bars) and the single set of parameters from global fitting at both flow durations (dotted bars). Effective on-rate, K_{on}^c, is calculate as $K_b^c - k_{off}^c$. Data are presented as the means ± SE of kinetic parameters.

Fig. 6. Dependence of cellular kinetic rates on flow rate. Lumped binding rate, K_b^c, and off-rate per cell, k_{off}^c, are the mean values of two sets of parameters from individual fitting at two flow durations of 10 and 15 min using Eqs. (2c) and (3b) at 1 (open bars), 5 (solid bars), and 10 (hatched bars) μl/min. Data are presented as the means ± SE of kinetic parameters. The P value indicates the level of statistical significance of differences in kinetic parameters at different flow rates.

using individual fitting at two flow durations ($K_b^c = 4.4 \times 10^{-3}$ and $k_{off}^c = 8.7 \times 10^{-4}$ s^{-1}). Effective on-rate, K_{on}^c, was then calculated ($= K_b^c - k_{off}^c$) and is illustrated in Fig. 5. Similar independence of flow duration was obtained at flow rates of 1 and 10 μl/min (data not shown). These results suggested that flow duration does not affect cellular kinetic parameters even though peak RU^P increased with duration, as was expected.

Similarly, the impact of flow rate on fitted kinetic parameters was further tested. To conduct a statistical t test, mean kinetic parameters obtained from the above individual fitting (cf. hatched bars in Fig. 5) were used. As exemplified in Fig. 6, lumped binding rate, K_b^c, was 2.4- and 2.6-fold lower at 1 μl/min (open bars) than at 5 (solid bars) and 10 (hatched bars) μl/min (1.8, 4.4, or 4.7×10^{-3} s^{-1}, $P = 0.024$ and 0.081, respectively), indicating that cell binding was regulated by flow rate. By contrast, off-rate per cell, k_{off}^c, was the same at 1, 5, and 10 μl/min ((7.9, 8.7, or $8.1) \times 10^{-4}$ s^{-1}, $P = 0.51$ and 0.69, respectively), indicating the characteristic time constant of bound RBCs debinding from the surface, $1/k_{off}^c \sim 1.2 \times 10^3$ s. Again, effective on-rate, K_{on}^c, was calculated and is also illustrated in Fig. 6. Flow rate, but not flow duration, regulated the binding of BSA-coupled RBCs to anti-BSA mAb-immobilized surface.
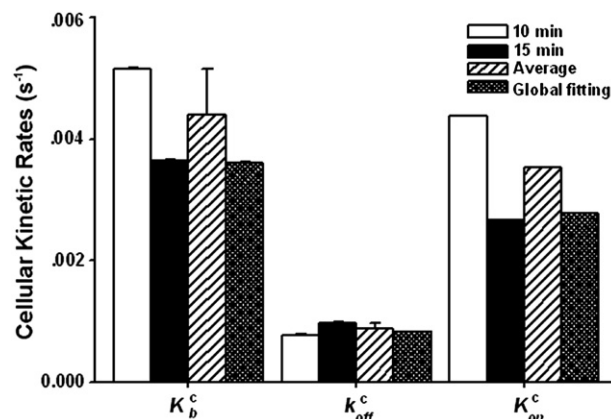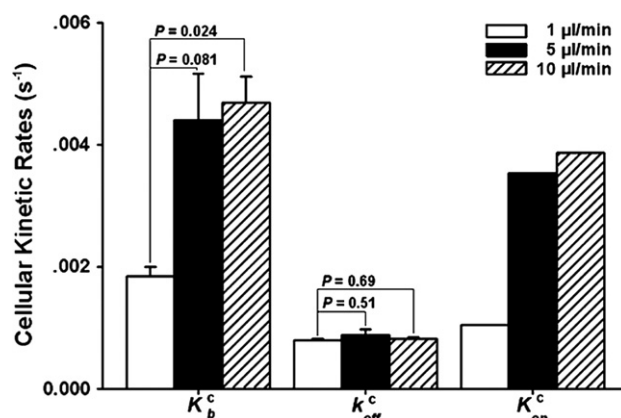
Kinetic parameters were also manipulated by molecular site densities

We further tested the effect of BSA site density (m_r) on cellular kinetic parameters. Two site densities of 45 and 82 μm^{-2} for BSA-coupled RBCs were used to conduct the measurements at 1 μl/min. As exemplified in Fig. 7, lumped binding rate, K_b^c, was 1.5-fold lower at 45 μm^{-2} (open bars) than that at 82 μm^{-2} (solid bars) (2.0 and 2.9×10^{-3} s^{-1}, respectively) (Fig. 7). By contrast, off-rate per cell, k_{off}^c, was similar at 45 and 82 μm^{-2} (7.7 and 9.3×10^{-4} s^{-1}, respectively). Again, effective on-rate, K_{on}^c, was calculated and is illustrated in Fig. 7. These data demonstrated that cell binding depends on site densities of interacting molecules.

Discussion

The goal of the current study was to quantify the binding kinetics of surface-bound molecules using surface plasmon resonance technique. We developed a cellular kinetic model to predict kinetic rates and binding affinity from sensorgrams measured using the
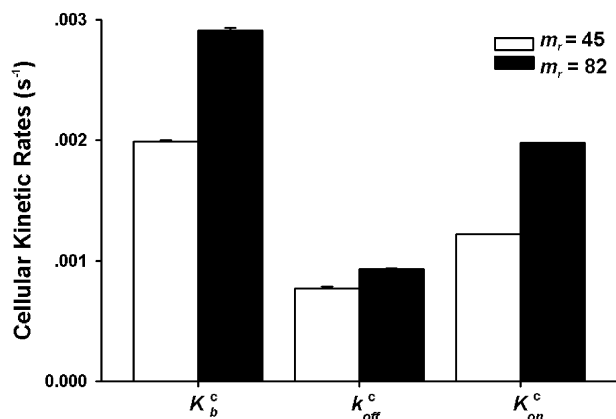
Fig. 7. Dependence of cellular kinetic rates on site density (m_r). Lumped binding rate, K_b^c, and off-rate per cell, k_{off}^c, are the kinetic parameters from individual fitting at a flow duration of 10 min using Eqs. (2c) and (3b) at BSA site densities of 45 (open bars) and 82 (solid bars) μm^{-2} at a given flow rate of 1 μl/min. Data are presented as the means ± SE of kinetic parameters.

Biacore biosensor. On development of the kinetic model with relevant experimental procedures and data analyses, we are able to characterize how flow dynamics affects the binding of cell-bound antigens (or receptors) to surface-immobilized antibodies (or ligands), and to determine how fast and how strong they bind, as well as how long they remain bound. Our data indicate that the model fits the sensorgram data well over systematically varied flow durations, flow rates, or site densities of BSA (Figs. 3–7). The advantage of the new approach is that it extends SPR technique from soluble analytes to cell-bound biomolecules with quantification of kinetic rates as well as binding affinity, which is crucial to understand the underlying mechanisms in such biological process as inflammatory cascade [32], tumor metastasis [33], and atherosclerosis and wound healing [34]. Such a new approach also provides a quantitative cell binding platform for the pharmaceutical industry.

BSA–anti-BSA mAb interaction is a typical molecular system used in developing bioanalytical and immunological methods. In the current work, we also measured 3D kinetic rates of binding of soluble BSA to anti-BSA mAb immobilized on chip surface at a flow rate of 30 μl/min and flow duration of 5 min. This yielded 3D on- and off-rates of 1.4×10^3 M^{-1} s^{-1} and 1.8×10^{-4} s^{-1}, respectively, or a 3D association constant of 0.8×10^7 M^{-1}, which is consistent with the 1.1×10^7 M^{-1} published previously [35]. It was also evident that the 3D off-rate so measured is comparable to the 2D off-rate obtained in the current work (7.9–8.7×10^{-4} s^{-1}) when taking into consideration the effect of anchorage of BSA molecules on RBC surface and the difference between BSA concentration in solution and BSA site density on RBCs. A one-order-of-magnitude lower off-rate per cell (2×10^{-5} s^{-1}) was obtained when malignant epithelial cells were driven to bind with immobilized peptides where a different molecular system was used in a similar Biacore cell assay [13]. Direct comparison of the 2D effective on-rate with the 3D on-rate is impossible, as they follow distinctive kinetic mechanisms.

Binding of cell-bound antigens (or receptors) to surface-immobilized antibodies (or ligands) under applied flow is a complicated biological and biophysical process. Flow has dual functionality: (1) to drive antigen- or receptor-bound cells to the vicinity of the chip surface, and to let them collide and interact with immobilized antibodies or ligands to form antigen–antibody or receptor–ligand bonds; and (2) to force the dissociation of formed bonds and to detach bound cells from surface. It was well understood that more

cells were captured on the chip surface with longer flow durations at a given flow rate. This would not affect binding kinetics per cell in the case where the number of bound cells is not geometrically saturated at a given site density of BSA molecules on chip surface (Figs. 3 and 5). It should be pointed out that such the cell binding would be unstable when flow duration is too short at a low flow rate (data not shown), as is expected.

Flow rate, however, does affect the effective on-rate $K_{on}^c (= k_{on}^c \times C)$, as the average concentration of freely flowing cells close to the surface ($\sim$one cell height high from the surface), C, is physically related to flow rate. Prediction of spatial and temporal distribution of flowing cells in a high bulk concentration of cells (e.g., 4×10^7 cells/ml in the current work) is a challenge even in fluid mechanics analysis, which is beyond the scope of the current work. Nevertheless, it seems reasonable to assume that C approximates the bulk concentration of flowing cells along the following lines of reasoning. In a typical CM5 chip (as seen in Fig. 1), the height of the flow chamber is approximately threefold higher (20 μm) than cell diameter ($\sim$6.5 μm), which confines the concentration gradient of flowing cells along the height. It takes $\sim$0.5–0.05 s for RBCs to flow from the inlet through the outlet of the chamber at flow rate of 1–10 μl/min, suggesting that sedimentation of flowing RBCs can be neglected. The total number of cells flowing into the chamber (2–60×10^5 cells) is at least 10 times higher than the number of bound cells geometrically available, N_{max} ($<10^4$ cells), which reduces the concentration gradient of flowing cells distributed from the center to the wall of the chamber. Taken together, it is possible to estimate on-rate per cell using $k_{on}^c \approx K_{on}^c/C$, which is 2.6, 8.8, and 9.7×10^{-11} ml · s^{-1} at 1, 5, and 10 μl/ml, respectively. Here, the differences in k_{on}^c are attributed mainly to the impact of different applied flows (or forces) on bond formation and dissociation per cell at different flow rates.

In addition to the estimated cellular kinetic rates, we were also able to obtain R_{max}, the RU value for the maximum number of bound cells available at a given chip surface, by fitting the sensorgrams using Eq. (2c). In the current work, R_{max} was predicted to be 137 ± 34.1, 102 ± 16.1, and 107 ± 9.4 RU at flow rates of 1, 5, and 10 μl/ml, respectively, and no statistical differences were found between any two estimated R_{max} values ($P > 0.4$). Here it is hard to measure R_{max} experimentally via saturating chip surface using BSA-coated RBCs, as the bound cells are difficult to remove completely and the interactions between free and bound cells and the RU fluctuation become much higher at the end of the sample injection phase. This would be even worse when high cell concentrations are used, where the model proposed would no longer applicable.

BSA site density also regulates cell binding. We estimated on-rate per cell, k_{on}^c, to be 3.1 and 4.0×10^{-11} ml · s^{-1} at BSA site densities of 45 and 82 μm^{-2}, respectively, at 1 μl/min (cf. Fig. 7). Such a difference may be interpreted from the viewpoint of 2D kinetics per molecule. In fact, the binding of an antigen- or receptor-bound cell is governed by intrinsic 2D kinetic rates and binding affinity per molecule, molecular site densities on cell and chip surfaces, collision frequency, and contact duration between two apposing surfaces, and applied force exerted from flow onto cells, as well as interactions among cells in a large population [18–20,23]. Even with the same intrinsic 2D kinetic rates and binding affinity per interacting molecule, 2D on-rate per cell was enhanced when the higher site density was used (Fig. 7). This enhancement could be saturated when saturated immobilization of anti-BSA mAb (e.g., from 9000 to 12,000 RU in the current work) is used (data not shown). Here the purpose of using a high-site-density anti-BSA mAb surface is to obtain the measurable RU and to retain the reasonable sensitivity of a cell binding assay. Such a high site density of anti-BSA mAb would not bias the 2D kinetic analysis, as only a few BSA molecules coupled to the RBC membrane and facing the

chip surface are geometrically available to interact with immobilized mAbs. For example, at the given BSA-coupled site densities of m_r = 45 and 82 μm^{-2} in the current work, the numbers of BSA molecules geometrically available to bind to immobilized mAbs are estimated to be ~207 and ~377, which follows the assumption that this reaction system is a small system, as compared with micromolar or nanomolar soluble BSA concentrations in 3D kinetic measurements, and retains the stochastic nature of 2D kinetic analysis. To further elucidate the molecular mechanism governing the binding of flowing cells to a surface, a molecular kinetic model that correlates 2D kinetics per cell with 2D kinetics per molecule is required, which is the ongoing work of our serial studies.

Finally, we developed a cellular kinetic model to quantify the kinetic parameters of surface-bound molecules obtained with the SPR technique. Relevant experimental procedures and data analysis were proposed. This new assay is able to be extended to other biological systems where interacting molecules are constitutively expressed or reconstructed on the surfaces of cells or other molecular carriers. Understanding the 2D cellular kinetics (the current work) and the 2D molecular kinetics (the ongoing project) is helpful in extending the SPR-based biosensor from measuring the kinetics of soluble molecules to measuring the kinetics of surface-bound molecules, which are important in clinical diagnosis and prognosis as well as in the pharmaceutical industry. And developing a kinetic model that correlates 2D and 3D kinetics of interacting molecules would further theoretical understanding of the binding kinetics of biomolecular interactions.

Acknowledgments

References

[1] D.G. Myszka, T.A. Morton, M.L. Doyle, I.M. Chaiken, Kinetic analysis of a protein antigen–antibody interaction limited by mass transport on an optical biosensor, Biophys. Chem. 64 (1997) 127–137.

[2] J.G. Quinn, R. O'Kennedy, Biosensor-based estimation of kinetic and equilibrium constants, Anal. Biochem. 290 (2001) 36–46.

[3] P.S. Katsamba, I. Navratilova, M. Calderon-Cacia, L. Fan, K. Thornton, M. Zhu, T.V. Bos, C. Forte, D. Friend, I. Laird-Offringa, G. Tavares, J. Whatley, E. Shi, A. Widom, K.C. Lindquist, S. Klakamp, A. Drake, D. Bohmann, M. Roell, L. Rose, J. Dorocke, B. Roth, B. Luginbuhl, D.G. Myszka, Kinetic analysis of a high-affinity antibody/antigen interaction performed by multiple Biacore users, Anal. Biochem. 352 (2006) 208–221.

[4] S.A. Hardy, N.J. Dimmock, Valency of antibody binding to enveloped virus particles as determined by surface plasmon resonance, J. Virol. 77 (2003) 1649–1652.

[5] P. Leonard, S. Hearty, J. Brennan, L. Dunne, J. Quinn, T. Chakraborty, R. O'Kennedy, Advances in biosensors for detection of pathogens in food and water, Enzyme and Microbial Technol. 32 (2003) 3–13.

[6] P. Skottrup, S. Hearty, H. Frokiaer, P. Leonard, J. Hejgaard, R. O'Kennedy, M. Nicolaisen, A.F. Justesen, Detection of fungal spores using a generic surface plasmon resonance immunoassay, Biosens. Bioelectron. 22 (2007) 2724–2729.

[7] M. Fivasha, E.M. Towlerb, R.J. Fisher, Biacore for macromolecular interaction, Curr. Opin. Biotechnol. 9 (1998) 97–101.

[8] R.l. Rich, D.G. Myszka, Survey of the year 2004 commercial optical biosensor literature, J. Mol. Recognit. 18 (2005) 431–478.

[9] R.L. Rich, D.G. Myszka, Survey of the year 2005 commercial optical biosensor literature, J. Mol. Recognit. 19 (2006) 478–534.

[10] J.G. Quinn, R. O'Kennedy, M. Smyth, J. Moulds, T. Frame, Detection of blood group antigens utilising immobilised antibodies and surface plasmon resonance, J. Immunol. Methods 206 (1997) 87–96.

[11] J.G. Quinn, S. O'Neill, A. Doyle, C. McAtamney, D. Diamond, B.D. MacCraith, R. O'Kennedy, Development and application of surface plasmon resonance-based biosensors for the detection of cell–ligand interactions, Anal. Biochem. 281 (2000) 135–143.

[12] S. Hearty, P. Leonard, J. Quinn, R. O'Kennedy, Production, characterisation and potential application of a novel monoclonal antibody for rapid identification of virulent *Listeria monocytogenes*, J. Microbiol. Methods 66 (2006) 294–312.

[13] S. Aggarwal, S. Janssen, R.M. Wadkins, J.L. Harden, S.R. Denmeade, A combinatorial approach to the selective capture of circulating malignant epithelial cells by peptide ligands, Biomaterials 26 (2005) 6077–6086.

[14] D. Hans, P. Pattnaik, A. Bhattacharyya, A.R. Shakri, S.S. Yazdani, M. Sharma, H. Choe, M. Farzan, C.E. Chitnis, Mapping binding residues in the *Plasmodium vivax* domain that binds Duffy antigen during red cell invasion, Mol. Microbiol. 55 (2005) 1423–1434.

[15] S.D. Holmes, K. May, V. Johansson, F. Markey, I.A. Critchley, Studies on the interaction of *Staphylococcus aureus* and *Staphylococcus epidermidis* with fibronectin using surface plasmon resonance, Biacore 28 (1997) 77–84.

[16] R.J. Fisher, F. Matthew, C.-F. Jose, B. Sharon, L.M. Karen, Real-Time Biacore measurements of *Escherichia coli* single-stranded DNA binding (SSB) protein to polydeoxythymidylic acid reveal single-state kinetics with steric cooperativity, Methods 6 (1994) 121–133.

[17] S.E. Chesla, P. Selvaraj, C. Zhu, Measuring two-dimensional receptor–ligand binding kinetics by micropipette, Biophys. J. 75 (1998) 1553–1572.

[18] M. Long, H.L. Goldsmith, D.F. Tees, C. Zhu, Probabilistic modeling of shear-induced formation and breakage of doublets cross-linked by receptor–ligand bonds, Biophys. J. 76 (1999) 1112–1128.

[19] M. Long, J. Chen, N. Jiang, P. Selvaraj, R.P. McEver, C. Zhu, Probabilistic modeling of rosette formation, Biophys. J. 91 (2006) 352–363.

[20] J. Huang, J. Chen, S.E. Chesla, T. Yago, P. Mehta, R.P. McEver, C. Zhu, M. Long, Quantifying the effects of molecular orientation and length on two-dimensional receptor–ligand binding kinetics, J. Biol. Chem. 279 (2004) 44915–44923.

[21] N. Zhang, M.H. Ahsan, L. Zhu, L.C. Sambucetti, A.F. Purchio, D.B. West, NF-kappaB and not the MAPK signaling pathway regulates GADD45beta expression during acute inflammation, J. Biol. Chem. 280 (2005) 21400–21408.

[22] T.E. Williams, S. Nagarajan, P. Selvaraj, C. Zhu, Concurrent and independent binding of Fcgamma receptors IIa and IIIb to surface-bound IgG, Biophys. J. 79 (2000) 1867–1875.

[23] L. Wu, B. Xiao, X. Jia, Y. Zhang, S. Lu, J. Chen, M. Long, Impact of carrier stiffness and microtopology on two-dimensional kinetics of P-selectin and P-selectin glycoprotein ligand-1 (PSGL-1) interactions, J. Biol. Chem. 282 (2007) 9846–9854.

[24] J. Lou, T. Yago, A.G. Klopocki, P. Mehta, W. Chen, V.I. Zarnitsyna, N.V. Bovin, C. Zhu, R.P. McEver, Flow-enhanced adhesion regulated by a selectin interdomain hinge, J. Cell. Biol. 174 (2006) 1107–1117.

[25] T. Yago, V.I. Zarnitsyna, A.G. Klopocki, R.P. McEver, C. Zhu, Transport governs flow-enhanced cell tethering through L-selectin at threshold shear, Biophys. J. 92 (2007) 330–342.

[26] Pharmacia Biosensor, Biomolecular interaction analysis with cells and vesicles, NIA Technology Note 105, Pharmacia Biosensor AB, 1975.

[27] L. Chiarantini, M. Magnani, Methods in molecular biotechnology, Humana Press, Totowa, N.J., 1996. pp. 143–192.

[28] M. Magnani, L. Chiarantini, E. Vittoria, U. Mancini, L. Rossi, A. Fazi, Red blood cells as an antigen-delivery system, Biotechnol. Appl. Biochem. 16 (1992) 188–194.

[29] G.P. Samokhin, M.D. Smirnov, V.R. Muzykantov, S.P. Domogatsky, V.N. Smirnov, Red blood cell targeting to collagen-coated surfaces, FEBS Lett. 154 (1983) 257–261.

[30] U.J. Dumaswala, R.U. Dumaswala, D.S. Levin, T.J. Greenwalt, Improved red blood cell preservation correlates with decreased loss of bands 3, 4.1, acetylcholinesterase, and lipids in microvesicles, Blood 87 (1996) 1612–1616.

[31] U.J. Dumaswala, M.J. Wilson, T. Jose, D.L. Daleke, Glutamine- and phosphate-containing hypotonic storage media better maintain erythrocyte membrane physical properties, Blood 88 (1996) 697–704.

[32] T.A. Springer, Traffic signals on endothelium for lymphocyte recirculation and leukocyte emigration, Annu. Rev. Physiol. 57 (1995) 827–872.

[33] S.M. Albelda, Role of integrins and other cell adhesion molecules in tumor progression and metastasis, Lab Invest. 68 (1993) 4–17.

[34] F. Grinnell, Wound repair, keratinocyte activation and integrin modulation, J. Cell. Sci. 101 (1992) 1–5.

[35] G. Li, X. Zhou, Y. Wang, A. El-Shafey, N.H. Chiu, I.S. Krull, Capillary isoelectric focusing and affinity capillary electrophoresis approaches for the determination of binding constants for antibodies to the prion protein, J. Chromatogr. A 1053 (2004) 253–262.